Supporting Information

The N-anchoring effect in NH_2-functionalized MOF-derived iron-carbon nanomaterials for oxygen reduction

Yanqiong Shen,[b,#] Lujiao Mao,[a,#] Rong Lin,[a] Qipeng Li,[b,*] and Jinjie Qian[a,*]

[a]Key Laboratory of Carbon Materials of Zhejiang Province, College of Chemistry and Materials Engineering, Wenzhou University, Wenzhou 325035, Zhejiang, P. R. China

[b]College of Chemistry and Chemical Engineering, Zhaotong University, Zhaotong 657000, Yunnan, P. R. China

[#]These authors contributed equally to this work.

*Corresponding author

E-mail: qpli@ztu.edu.cn (Q. Li); jinjieqian@wzu.edu.cn (J. Qian)

Number of pages: 31 (S1-S31)

Number of tables: 6 (Table S1-Table S6)

Number of figures: 16 (Figure S1- Figure S16)

Table of contents

Experimental Section

Materials

The following chemicals and solvents are purchased and used without further purification. Zinc nitrate hexahydrate ($Zn(NO_3)_2 \cdot 6H_2O$, 99.9% metals basis, Aladdin), Iron nitrate nonahydrate ($Fe(NO_3)_3 \cdot 9H_2O$, 99.9% metals basis, Aladdin), 2-Aminoterephthalic acid ($H_2BDC\text{-}NH_2$, AR, 98.0%, Aladdin), Terephthalic acid (H_2BDC, AR, 98.0%, Aladdin), Polyvinylpyrrolidone (PVP, 99.0%, 58,000, Aladdin), JM 20 wt% Pt/C (HISPEC 3000), Potassium hydroxide (KOH, AR, 90.0%, Aladdin), N,N-dimethylformamide (DMF, AR, 99.5%, Aladdin), Ethanol (EtOH, AR, ≥99.5%, Aladdin), Distilled water, and Nafion solution (5 wt %, Dupont).

Syntheses of MOF-5-NH_2 and MOF-5

Initially, 250 mg of polyvinylpyrrolidone (PVP, 58,000) was fully dissolved in a mixture of 5 mL EtOH and 5 mL of DMF, subsequently, heated at 130 °C for 15 min in open air with a stirring speed of 500 rpm. Subsequently, 5 mL of DMF solution containing $Zn(NO_3)_2 \cdot 6H_2O$ (300 mg) and $H_2BDC\text{-}NH_2$ (75 mg) was introduced into the above solution, and the reaction proceeded at 130 °C for 2 h. The synthesis of MOF-5 diverged from that of MOF-5-NH_2 solely in substituting H_2BDC for $H_2BDC\text{-}NH_2$. In this study, MOF-5 was synthesized by substituting $H_2BDC\text{-}NH_2$ with H_2BDC, based on the introduced organic ligands. The yield of MOF-5-NH_2 in this study was approximately 48%, contingent upon the organic ligand utilized.

Syntheses of MOF5A-Fe@NC and MOF5-Fe@C

Add 30 mg of MOF-5-NH_2 to 5 mL of ethanol solution containing 5 mg of $Fe(NO_3)_3 \cdot 9H_2O$, and stir at 400 rpm for 24 h. Subsequently, calcinate at 900 °C with a heating rate of 10 °C min^{-1} for 2 h in an argon tube furnace to produce MOF5A-Fe@NC. The synthesis of MOF5-Fe@C follows the same procedure, with the substitution of MOF-5 for MOF-5-NH_2. The synthesis of MOF-derived carbon nanomaterials demonstrates high reproducibility, with MOF5A-Fe@NC retaining approximately 31% of its initial mass after carbonization at 900 °C. Hereinafter referred to as Fe@NC and Fe@C.

Material characterization

The morphology and structure of all the samples were examined using a scanning electron microscope (SEM, JEOL JSM-6700FA). The Powder X-ray diffraction (PXRD) pattern of the products was collected at room temperature using a Bruker (Karlsruhe, Germany) D8 Advance powder diffractometer operating at 40 kV and 40 mA for graphite monochromatized Cu Kα radiation (λ = 1.54 Å), with a scan speed of 10° min^{-1} and a step size of 0.025°. Fourier Transform Infrared (FT-IR) spectra were obtained using a PerkinElmer Frontier MIR type spectrometer. The thermal stability of the crystal was tested by thermogravimetric analysis (TGA) with a differential scanning calorimeter (DSC, Netzsch STA 449 C), using a heating rate of 10 °C min^{-1} under the nitrogen atmosphere. The N_2 adsorption study was conducted in the Specific Surface Area & Pore Size Analyzer (BSD-PS1 by BSD Instrument), where the

samples, after being activated at high temperatures, were placed in a clean ultra-high vacuum system at the cryogenic temperature of 77 K. Transmission electron microscope (TEM, JEOL JEM-2100F microscope), high-resolution transmission electron microscope (HR-TEM), elemental mapping, and energy dispersive X-ray spectroscopy (EDX) analyses were employed to characterize the structures and properties. The Raman spectrometer (LabRAM HR Evolution) can be used to study the molecular structure of materials at GS1000. Finally, the chemical characteristics of Fe@NC and Fe@C compounds were collected using X-ray photoelectron spectroscopy (XPS, Thermo Scientific ESCALAB 250).

Electrochemical measurements

The electrochemical tests were performed on the three-electrode Metrohm-Autolab (PGSTAT302N) utilizing a carbon rod and an Ag/AgCl electrode as the counter and reference electrodes, respectively. A glassy carbon rotating ring disk electrode (RRDE, diameter 5.6 mm) was employed as the working electrode for evaluating the ORR activity of these electrocatalysts, resulting in a catalyst loading of 0.8 mg cm^{-2}. The electrocatalyst ink was prepared as follows: the as-synthesized catalyst powder (5 mg) was dispersed in a mixed solution of ethanol (300 μL), H_2O (150 μL), and Nafion solution (5 wt%, 50 μL). Subsequently, the mixture was ultrasonicated for 1 h to form a homogeneous ink. Subsequently, the electrocatalytic activities of catalysts toward ORR were measured at room temperature, and the measured potentials versus the reference electrode Ag/AgCl were converted to a reversible hydrogen electrode (RHE)

according to the Nernst equation:

$$E_{RHE} = E_{Ag/AgCl} + 0.059 \times pH + E^{\theta}_{Ag/AgCl}$$,where the $$E^{\theta}_{Ag/AgCl} = 0.198\ V$$

(1)

Cyclic voltammetry (CV) experiments were conducted with a scan rate of 10 mV s^{-1}, and the linear sweep voltammogram (LSV) curves were carried out at 5 mV s^{-1} under various rotation rates (100, 400, 900, 1600, and 2500 rpm) to obtain the polarization curves in N_2-/O_2-saturated 0.1 M KOH solution. The ORR reaction kinetics were evaluated using the Koutechy-Levich (K-L) equation:

$$\frac{1}{J} = \frac{1}{J_L} + \frac{1}{J_K} = \frac{1}{B\omega^{-1/2}} + \frac{1}{J_K} \quad (2)$$

$$J_L = 0.2nFC_0D_0^{2/3}v^{-1/6}\omega^{-1/2} = B\omega^{-1/2} \quad (3)$$

where J, J_L, and J_k represent the measured, diffusion-limiting, and kinetic current density, respectively; ω is the angular velocity of the electrode; n represents the number of electrons; F is the Faraday constant (F=96,485 C mol^{-1}); C_o is the saturated O_2 concentration (1.21×10^{-6} mol cm^{-3}); D_o is the diffusion coefficient of O_2 in 0.1 M KOH (1.9×10^{-5} cm^2 s^{-1}); ν is the kinematic viscosity (0.01 cm^2 s^{-1}).

The Tafel slopes were obtained from the LSV curves at 1600 rpm. To evaluate the relative electrochemically active surface areas of catalysts, the double-layer capacitance (C_{dl}) is estimated. The values of C_{dl} (mF cm^{-2}) are determined from the CV plots measured in the region from 0.99 to 1.09 V vs. RHE at various scan rates of 5, 10, 20, 40, and 80 mV s^{-1} in 0.1 M N_2-saturated KOH. By fitting the middle capacitive current density at the different scan rates, half of the slope of the plot

represents the value of C_{dl}. The A.C. impedance spectra were collected at frequencies ranging from 10^6 Hz to 0.01 Hz at 0.7 V vs. RHE. The following equations are used to calculate the number of electrons transferred (*n*) and the percentage of peroxide (HO_2^- %) released during ORR, based on the disk current (I_d) and ring current (I_r). Therein, the H_2O_2 collection coefficient (N) at the ring in RRDE experiments is 0.38.

$$n = \frac{4|I_d|}{|I_d| + I_r/N} \quad (4)$$

$$HO_2^-(\%) = \frac{2I_r/N}{|I_d| + |I_r|/N} \times 100\% \quad (5)$$

A chronoamperometry test was conducted at a constant potential of 0.45 V vs. RHE with a rotation rate of 1600 rpm and a constant O_2 flow. As for the methanol crossover study, the curves were recorded at the constant potential of 0.475 V vs. RHE with 14 mL of methanol being added to 100 mL of O_2-saturated electrolyte.

Zn-air battery

Disperse 5 mg of catalyst in a mixture of 500 μL ethanol and 50 μL Nafion to form a catalyst ink (the mass loading is calculated to be 1.0 mg cm^{-2}). For the primary battery, a carbon paper electrode with the obtained catalyst is used as a cathode, and a polished Zn foil is used as an anode, while the electrolyte is set to 6.0 M KOH. Zn-air batteries were evaluated under ambient conditions.

Structural Details

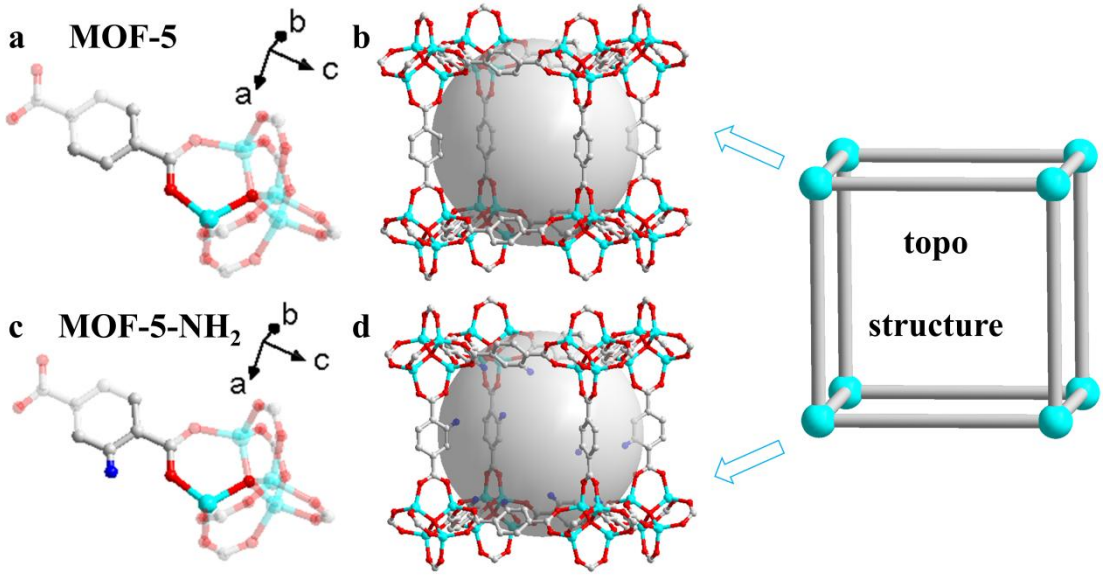

Figure S1. Compared to (a, b) pure MOF-5, (c, d) MOF-5-NH_2 retains the same topological features but differs in the presence of functional NH_2 groups.

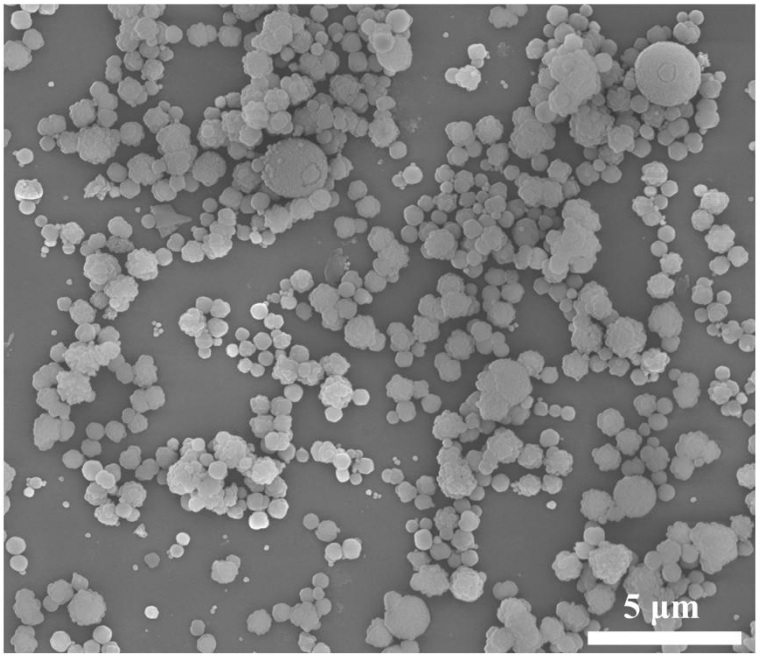

Figure S2. SEM image of MOF-5.

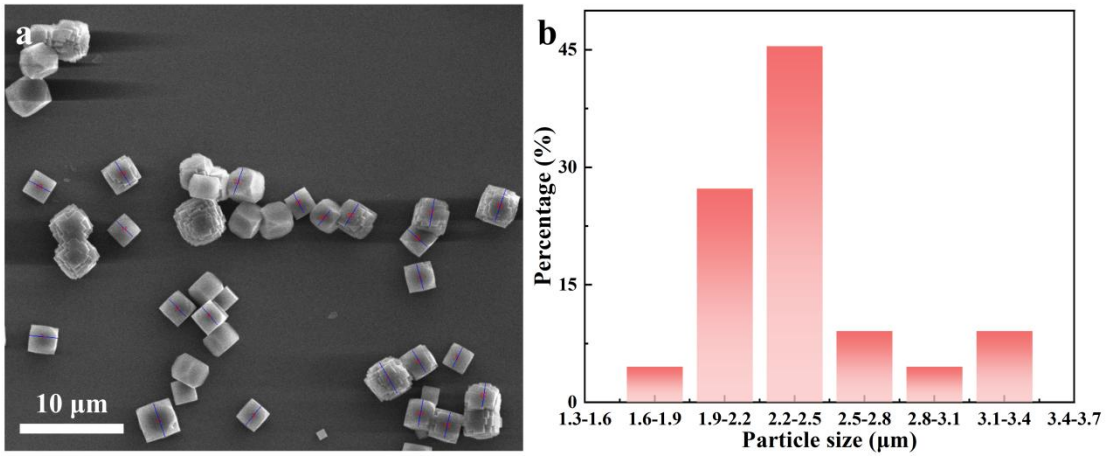

Figure S3. MOF-5-NH_2 with particles approximately 2.2 µm in size.

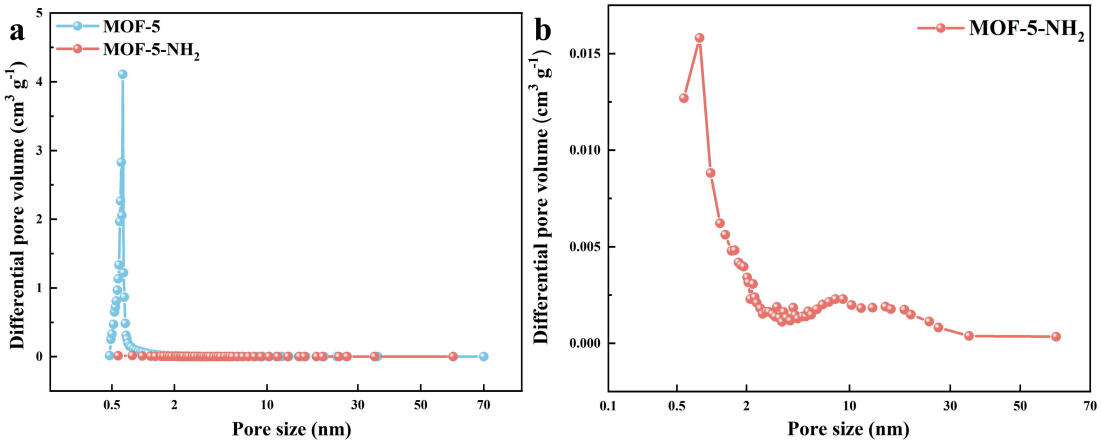

Figure S4. (a) The PSD analysis of MOF-5 and MOF-5-NH_2. (b) An enlarged view of PSD analysis of MOF-5-NH_2 within the range of 0.5 to 60 nm.

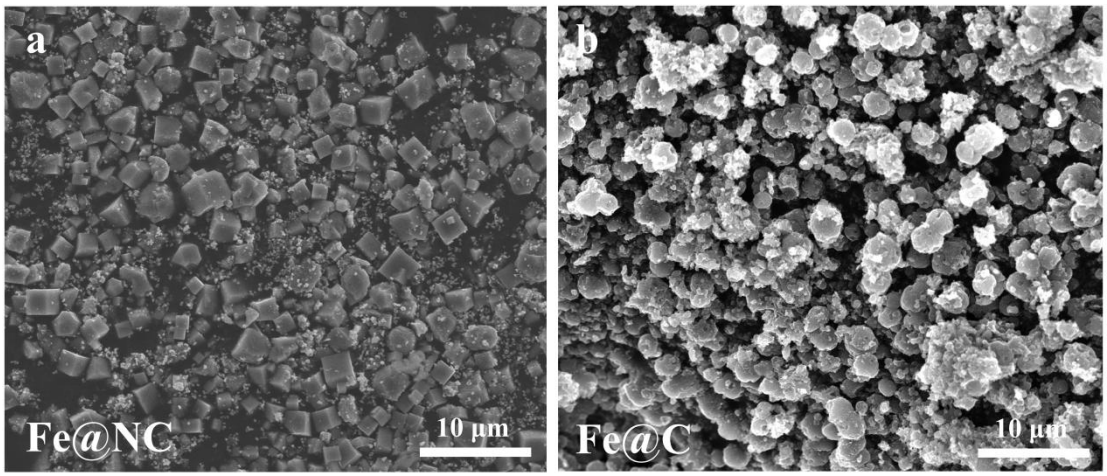

Figure S5. SEM images of (a) Fe@NC and (b) Fe@C.

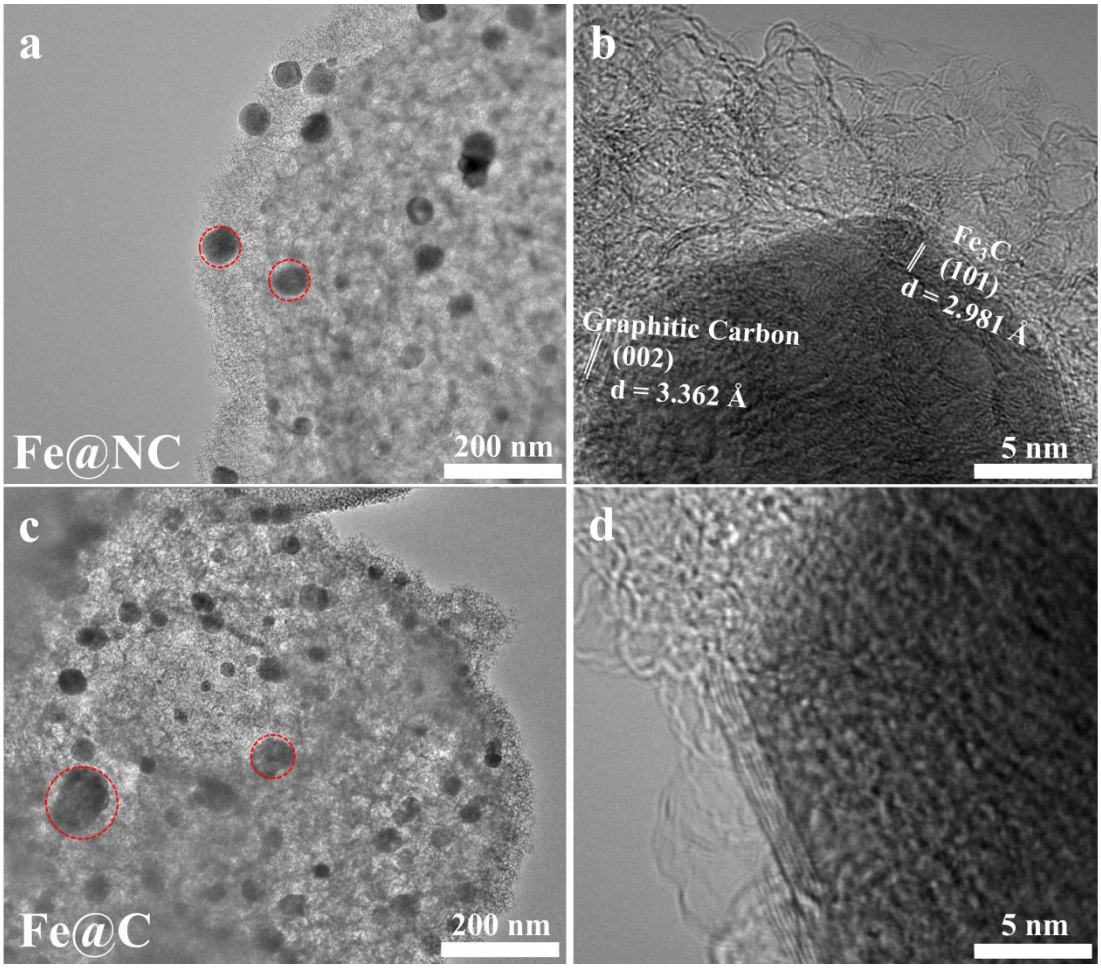

Figure S6. TEM and HR-TEM images of (a, b) Fe@NC and (c, d) Fe@C.

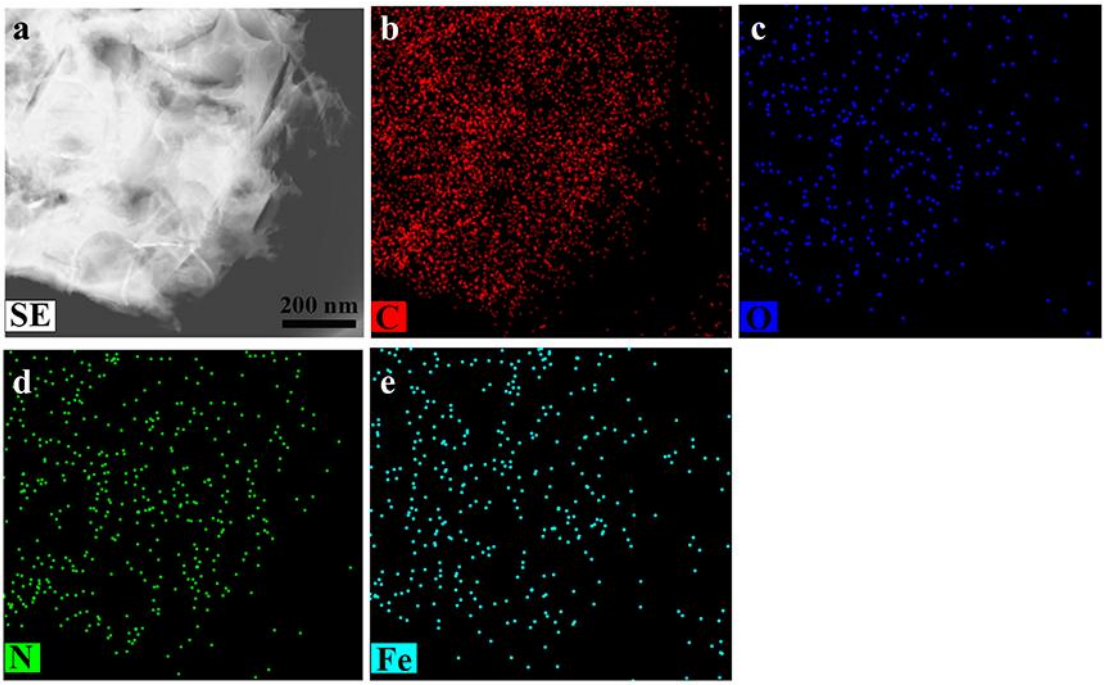

Figure S7. (a) HAADF-STEM and (b-e) element mapping images of Fe@NC.

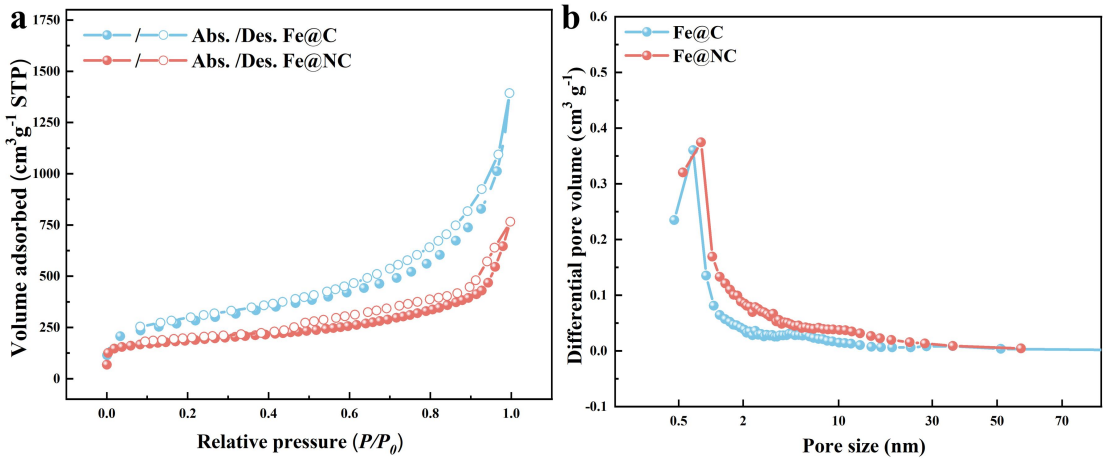

Figure S8. (a) N_2 isotherms, (b) PSD analysis of Fe@NC and Fe@C.

Additional Electrochemical Data

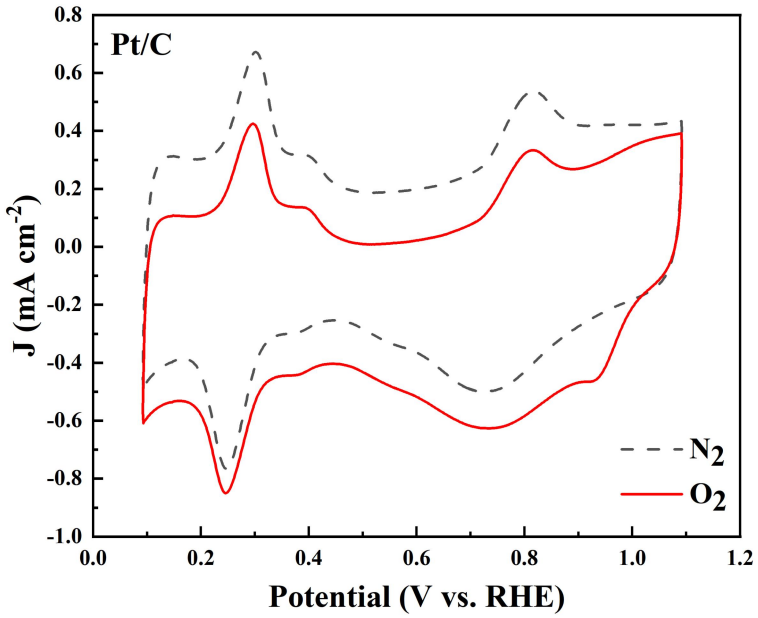

Figure S9. The CV curves of Pt/C in N_2-/O_2-saturated solutions.

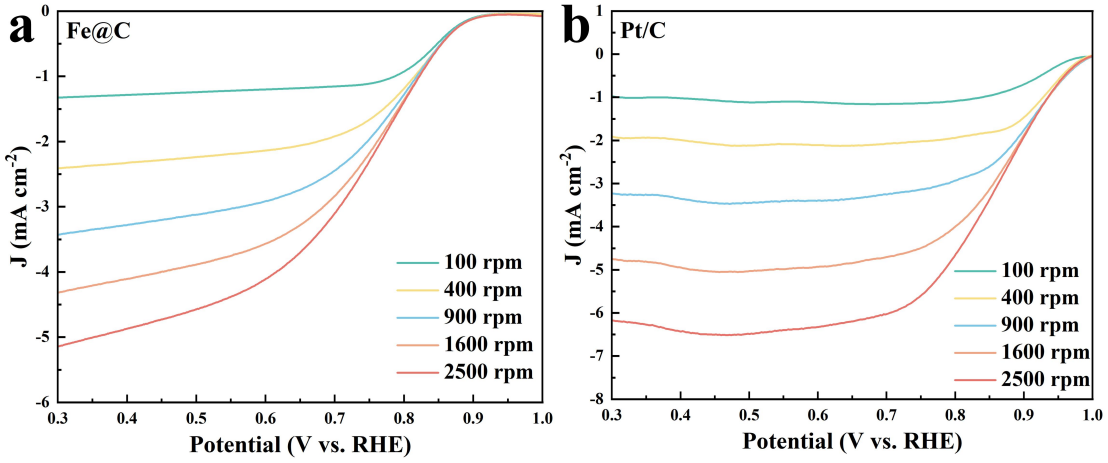

Figure S10. LSV curves at various rotating speeds from 100 to 2500 rpm of (a) Fe@C and (b) Pt/C.

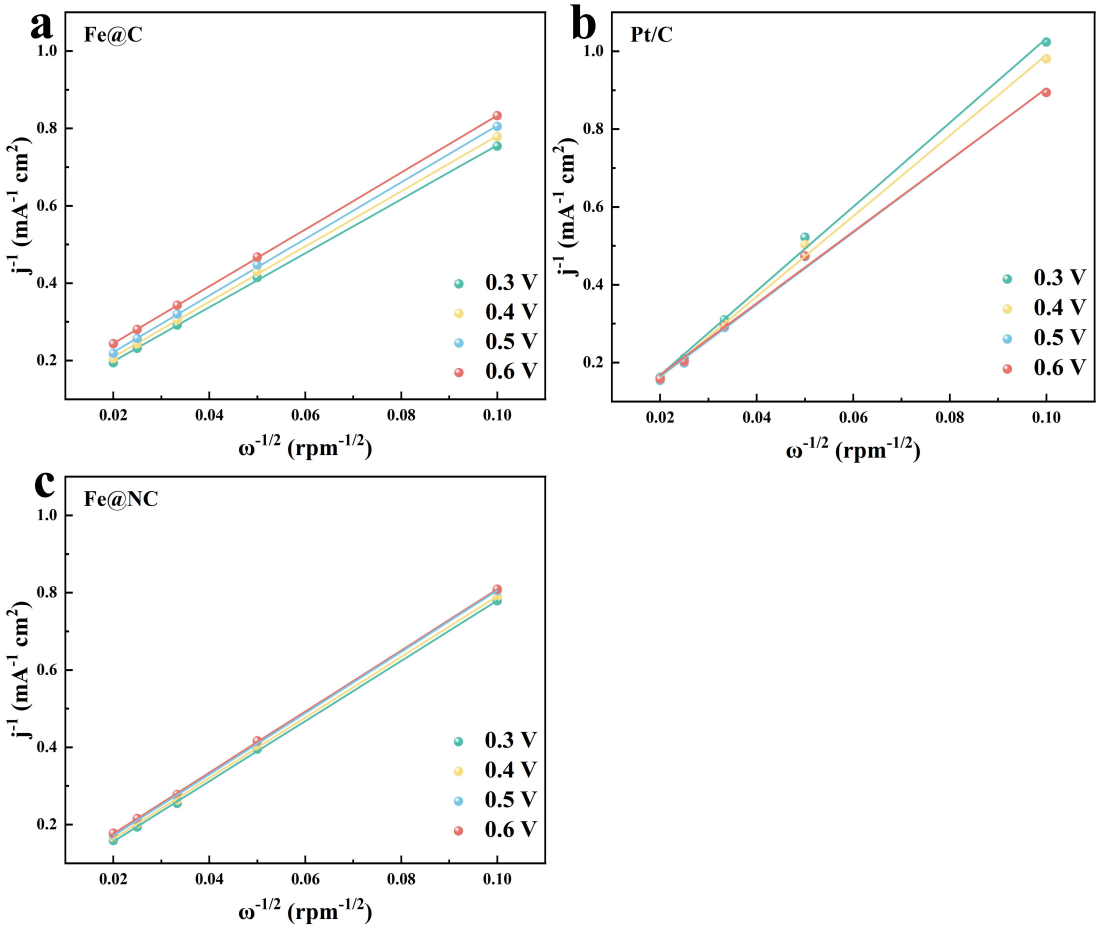

Figure S11. The K-L plots at various potentials from 0.3-0.6 V of (a) Fe@C, (b) Pt/C and (c) Fe@NC.

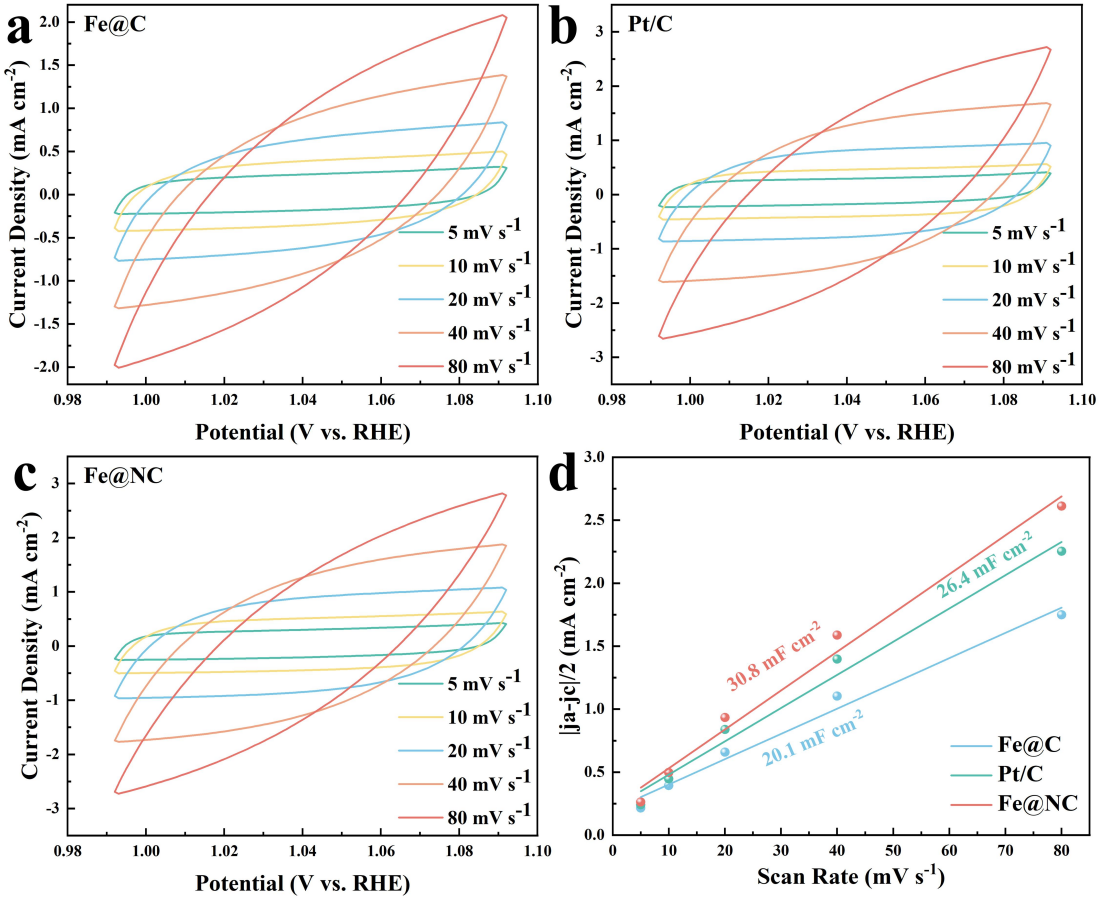

Figure S12. CV curves at different sweep speeds from 5 to 80 mV s^{-1} of (a) Fe@C, (b) Pt/C, (c) Fe@NC, (d) C_{dl} curves at 1.04 V.

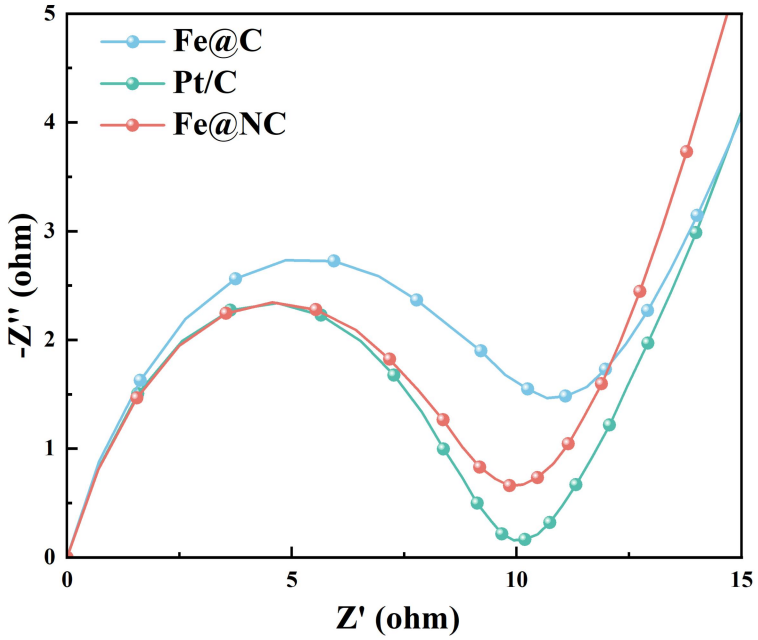

Figure S13. EIS plots of Fe@C, Pt/C and Fe@NC.

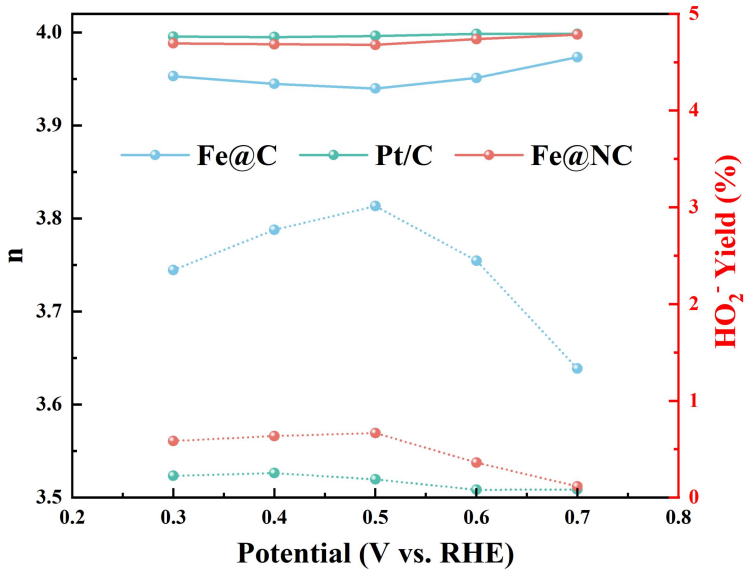

Figure S14. The *n* numbers and HO_2^- yields of Fe@C, Pt/C and Fe@NC.

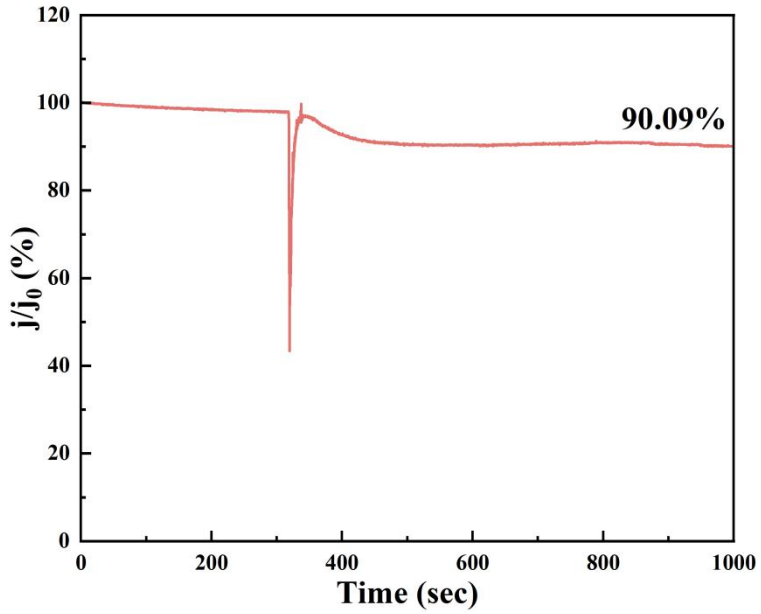

Figure S15. Anti-MeOH test of Fe@NC.

The **MOF5A-Fe@NC** catalyst exhibited a sudden drop in current density upon the addition of 3.0 M methanol at 300 seconds. This sharp decline is primarily attributed to the use of a small glass electrolytic cell during the test, which caused a significant instantaneous impact on the catalyst due to the rapid introduction of methanol. However, it was noted that the catalyst quickly recovered its original current within a short period, demonstrating its minimal sensitivity to methanol and excellent methanol tolerance.

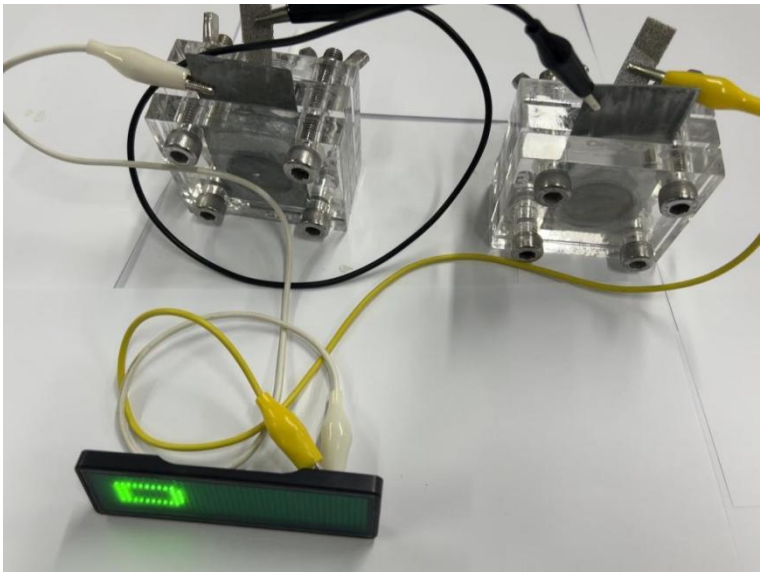

Figure S16. Two Zn-air batteries connected in series.

Additional Tables

Items	MOF-5[Ref.1]
Formula	$C_{24}H_{12}O_{13}Zn_4$
Mass	769.90
crystal system	Cubic
Space group	$Fm\bar{3}m(225)$
a(Å)	25.8919(4)
b(Å)	25.8919(4)
c(Å)	25.8919(4)
α(°)	90.00
β(°)	90.00
γ(°)	90.00
V(Å^3)	17357.7(5)
T(K)	100(2)
Z	8
F(000)	3040
R_{int}	0.0488
$R_1(I>2\sigma(I))$	0.1875
wR_2(all reflections)	0.2223

Table S1. Single Crystal X-Ray Data for MOF-5.

Ref.1: For more details on the crystal structure data, please see the previously published works, e.g. The Journal of Physical Chemistry C, 2010, 114, 16181-16186.

Items	**MOF-5-NH_2[Ref.2]**
Formula	$C_{27.90}H_{22.41}N_3O_{13.21}Zn_4$
Mass	872.54
crystal system	Block
Space group	$Fm\bar{3}m(225)$
a(Å)	25.7786(7)
b(Å)	25.7786(7)
c(Å)	25.7786(7)
α(°)	90.00
β(°)	90.00
γ(°)	90.00
V($Å^3$)	17130.8(8)
T(K)	200(2)
Z	8
F(000)	3492
R_{int}	0.0405
$R_1(I>2\sigma(I))$	0.1078
wR_2(all reflections)	0.1035

Table S2. Single Crystal X-Ray Data for MOF-5-NH_2.

Ref.2: For more details on the crystal structure data, please see the previously published works, e.g. Journal of the American Chemical Society, 2008, 130, 8508-8517.

Table S3. The BET Surface Area and Total Volume of the Samples by Nitrogen Adsorption and Desorption Measurement.

Samples	BET surface area ($m^2 g^{-1}$)	Total pore volume ($cm^3 g^{-1}$)
MOF-5	745.1930	0.4242
MOF-5-NH_2	39.3489	0.1458
Fe@C	950.7012	2.0087
Fe@NC	604.4494	1.1097

Table S4. Summary of Peak Position of XPS Binding Energy.

Elements	Formula	Binding Energy (eV)
C	C-C	284.8
	C-N	286.2
	C-O	287.6
	C=O	289.5
O	M-O	532.4
	C-O	533.4
N	pyridinic-N	399.1
	pyrrolic-N	400.5
	graphitic-N	401.5
	oxidized-N	403.0
Fe	Fe $2p_{1/2}$/Fe $2p_{3/2}$	707.2/720.2
	Fe-N_x	709.4/723.2
	Satellite	713.0/726.8

Table S5. The Composition and Deconvoluted Contents of the Catalysts Based on XPS & ICP Measurement.

Samples	XPS (At %)				
	C	O	N	Fe	Zn
Fe@NC	79.96	16.02	3.35	0.63	0.04
Fe@C	89.10	10.35	--	0.40	0.15

Samples	ICP (Wt %)
	Fe
MOF5A-Fe@NC	5.3
MOF5-Fe@C	2.8

Table S6. The ORR Performance Comparison of Various Electrocatalysts in Alkaline Solution.

Catalyst	E_{onset} (V vs. RHE)	$E_{1/2}$ (V vs. RHE)	$\|J_L\|^*$ (mA·cm^{-2})	Ref.
Fe@NC	0.972	0.855	4.815	
Fe@C	0.921	0.762	3.978	This Work
Pt/C	0.995	0.874	5.048	
FeN@FCS-900	0.93	0.78	-	[3]
N-Fe/G	0.93	0.83	6.49	[4]
FeS-FeNC@NSC	-	0.886	5.4	[5]
Fe-N_x-CNF	-	0.875	6.08	[6]
FeN/C_{60}O-900	0.98	0.85	5.23	[7]
F-N/$FeCoNC_{900}$	0.97	0.87	5.7	[8]
N-Fe/GC	0.93	0.83	6.49	[9]
Fe-CNSs-N	0.948	0.828	5.52	[10]
Zn0.22-FeNC	1.01	0.84	6.0	[11]
Fe/FeN@NC-2-800	0.873	0.813	6.04	[12]

*The limited current densities (J_L) are compared at a rotation speed of 1600 rpm unless otherwise state.

References:

[1] N. Lock, Y. Wu, M. Christensen, L. Cameron, V. Peterson, A. Bridgeman,C. Kepert and B. Iversen, Elucidating Negative Thermal Expansion in MOF-5, J. Phys. Chem. C, 2010, **114**, 16181-16186.

[2] K. Tanabe, Z. Wang, S. Cohen. Systematic Functionalization of a Metal-Organic Framework via a Postsynthetic Modification Approach, J. Am. Chem. Soc. 2008, **130**, 8508-8517.

[3] B. Jiang, S. Wang, F. Meng, L. Ju, W. Jiang, Q. Ji and H. Quan. Enhancing the ORR activity of fullerene-derived carbons by implanting Fe in assembled diamine-C_{60} spheres, CrystEngComm, 2022, **24**, 5783-5791.

[4] J. Wang, H. Zhang, C. Wang, Y. Zhang, J. Wang, H. Zhao, M. Cheng, A. Li, J. Wang. Co-synthesis of atomic Fe and few-layer graphene towards superior ORR electrocatalyst, Energy Storage Mater., 2018, **12**, 1-7.

[5] Z. Chen, R. Liu, S. Liu, J. Huang, L. Chen, R. Nadimicherla, D. Wu and R. Fu. FeS/FeNC decorated N,S-co-doped porous carbon for enhanced ORR activity in alkaline media, Chem. Commun., 2020, 56, 12921-12924.

[6] W. Miao, F. Huang, X. Shen, S. Li, X. Cao, X. Zhang, J. Yu and X. Dong. Single atom Fe-based catalyst derived from hierarchical (Fe,N)-ZIF-8/CNFs for high-efficient ORR activity, Mater. Chem. Front., 2022, **6**, 3213-3224.

[7] L. Ju, G. Hao, F. Meng, W. Jiang and Q. Ji. Nanoarchitectonics tuning for Fe/N-doped C_{60}-derived carbon electrocatalysts with enhanced ORR activity by oxygen plasma treatment on C_{60}, J. Mater. Chem. A, 2023, **11**, 25534-25544.

[8] X. He, L. Chang, H. Wu, G. Liu, Y. Zhang, A. Zhou. Design of ZIF-67-derived Fe, N and F co-doped porous carbon material and evaluation of its ORR and OER performance, J. Alloys Compd., 2023, **967**, 171709.

[9] S. Li, D. Zhang, X. Meng, Q. Huang , C. Sun, Z. Wang. A flexible lithium-ion battery with quasi-solid gel electrolyte for storing pulsed energy generated by triboelectric nanogenerator, Energy Storage Mater., 2018, **12**, 17-22.

[10] W. Cheng, P. Yuan, Z. Lv, Y. Guo, Y. Qiao, X. Xue, X. Liu, W. Bai, K. Wang, Q.

Xu, J. Zhang. Boosting defective carbon by anchoring well-defined atomically dispersed metal-N_4 sites for ORR, OER, and Zn-air batteries, Appl. Catal. B Environ. Energy, 2020, **260**, 11819.

[11] Y. Zhan, H. Zeng, T. Zhao, A. Situ, L. Yang, Z. Zhang, P. Li, Z. Wang, J. Wen, F. Xie, J. Chen, X. Tang, H. Meng. Densely accessible single atom Fe sites dispersed on porous carbon as highly stable and active ORR catalyst for PEMFC, Int. J. Hydrogen Energy, 2024, **56**, 1049-1056.

[12] C. Feng, Y. Guo, S. Qiao, Y. Xie, L. Zhang, L. Zhang, W. Wang, J. Wang. 2-Methylimidazole as a nitrogen source assisted synthesis of a nano-rod-shaped Fe/FeN@N-C catalyst with plentiful FeN active sites and enhanced ORR activity, Appl. Surf. Sci., 2020, **533**, 147481.